CHARACTERIZING THE MAGNETIZED TURBULENCE IN THE CENTRAL REGION OF SPIRAL GALAXY IC 342

by

Danielle Whitfield

Supervised by Dr. Martin Houde

Physics and Astronomy Department

The University of Western Ontario
London, Ontario, Canada

Acknowledgements

I would first and foremost like to thank my supervisor, Dr. Martin Houde, for giving me the opportunity to pursue this project. Thank you for your guidance, advice, and answers to my many questions throughout the course of this project.

I would also like to thank the professors in both the Physics & Astronomy and Writing departments at Western for all the skills and knowledge that I have gained during my undergraduate career. I deeply admire and respect the passion that you bring to your work and the enthusiasm with which you teach your classes.

To my family, for supporting me through my undergraduate years and allowing me to discover my own path. To my wonderful friends, both in and outside of the Physics department, for the infinite support and encouragement over the past five years. I could not have done this without you.

Abstract

We use previously published linearly polarized synchrotron emission data to perform a dispersion analysis with the aim of characterizing the magnetized turbulence in spiral galaxy IC 342. We consider two areas in the central region of the galaxy: the inner region of the upper source and the entire central region with the internal region of the upper source removed, and by using two computational programs in IDL we are able to produce plots of the dispersion and turbulent autocorrelation functions for each. We are able to discern a correlation length from the width of the autocorrelation function for the entire source, but not for the inner region of the upper source. We determine a turbulent correlation length of 144 ± 9 pc for the entire central region less the upper inner source and turbulent-to-ordered magnetic field strength ratio B_t/B_0 to be 0.70 ± 0.04. The field strength ratio suggests that the central region of the galaxy contains an ordered field that is relatively stronger than its turbulent field.

Keywords: galaxies: individual (IC 342), galaxies: spiral, turbulence, magnetic fields

Contents

List of Figures

List of Tables

Page

Chapter 1

Introduction

1.1 Magnetic Fields in Spiral Galaxies

All galaxies in the universe contain a magnetic field. This field can be separated into two components: an ordered and a turbulent component. In spiral galaxies, the ordered (or mean) field is typically found in close alignment with the spiral arms or slightly offset from the position of the arms (Phillips, 2005). Each of these arms possesses a pitch angle that measures the angle from a circle about the galactic center to the tangent of that particular spiral arm, which reveals how 'tightly wound' the spiral arms and the associated ordered fields of the galaxy are (Moss, 2012).

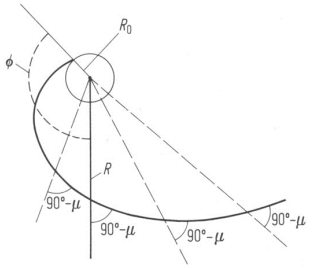

Figure 1.1: Graphic of a hyperbolic spiral arm trailing out from the galactic center (GC). The pitch angle is indicated by the variable μ, while ϕ is the winding angle; $90 - \mu$ is the characteristic angle; R is the radius from the center point to the tangent point on the spiral arm; and R_0 is the radius of the GC. Image source: https://ned.ipac.caltech.edu/level5/STRUCTURE/spst.html

The turbulent component consists of fluctuations that permeate the entire galaxy, as is found in the Milky Way (Sparke and Gallagher III, 2007). These fluctuations are caused by disruptions in the gas, for example, due to supernova explosions or through dynamo motion. A dynamo is a uniformly conducting, self-excited object that converts kinetic energy into magnetic energy. In this case we are considering small-scale dynamos, which are objects that are found in any sufficiently conductive plasma. These dynamos interact with eddies, which are regions where the vorticity, a measure of the rotation at any point, is non-zero (Yu, 2012; Ryden, 2011). The small-scale dynamos produce magnetic fields at scales that are smaller than the turbulent eddies. These dynamos can grow rapidly in the presence of the aforementioned eddies, which are a common occurrence in galaxies. Thus we expect to see these dynamos in galactic structures because the length scales of the turbulent motions are small enough to allow the dynamo action to propagate (Brandenburg, Sokoloff and Subramanian, 2012).

These small scale dynamos become excited when the magnetic Reynolds number exceeds a particular critical value. Brandenburg et al. (2012) define the magnetic Reynolds number as

$$Re_M = \frac{\mu_{rms}}{\eta k_f}, \tag{1.1}$$

where μ_{rms} is the root mean square of the turbulent velocity of the medium, η is the magnetic diffusivity, and k_f is the wave number corresponding to energy injection into the medium. Since the magnetic Reynolds number is directly proportional to the root mean square of the turbulent velocity, a high magnetic Reynolds number will also correspond to higher turbulence and an excitation in the small-scale dynamo (Brandenburg et al., 2012).

1.2 The Origin of Magnetic Fields

The origin of magnetic fields in galaxies has spurred several theories throughout history. One theory suggests the presence of seed fields, which are primordial magnetic fields that sweep up matter over time (Beck, 2016). In order for these seed fields to grow, there must be a source within the galactic dynamo that encourages amplification. The presence of vorticity as a result of the small-scale dynamo can provide the needed amplification, particularly in the ionized plasma of a galaxy, where the presence of vorticity is directly linked to the generation of magnetic fields (Widrow et al., 2012).

The generation of these seed fields has remained an unanswered question for many years, and many theories have been posed to suggest the origin of these fields. As Donnert, J. et al. (2008) note, there are three primary classes of theories for the creation of seed fields and their subsequent transformation into galactic magnetic fields. The first is the creation of a magnetic field through a dynamo, which is referred to as the 'Biermann battery effect' (Kulsrud et al., 1997; Ryu et al., 1998; Miranda et al., 1998; Hanayama et al., 2005). The second class considers magnetic fields as the product of primordial processes that took place in the early Universe, such as inflation (Tsagas, 2005), and the generation of turbulence by the small-scale dynamo in the radiation-dominated epoch of the early Universe (Wagstaff et al., 2014). The final set of theories considers magnetic fields as products of galactic winds (Bertone et al., 2006) or active galactic nuclei (Furlanetto and Loeb, 2001; Xu et al., 2010).

1.3 Magnetized Turbulence

Before we define magnetized turbulence, we will first investigate the general concept of turbulence and then apply it to magnetic fields in galaxies. In fluids, the motion of flows is governed by the Navier-Stokes equations:

$$\frac{\partial \mathbf{u}}{\partial t} + \mathbf{u} \cdot \nabla \mathbf{u} = -\frac{\nabla P}{\rho} + \nu \nabla^2 \mathbf{u}, \tag{1.2}$$

where $\mathbf{u}$ is the velocity of a particular piece of the fluid, P is the pressure in the fluid, ρ is the density of the fluid, and ν is the kinematic viscosity (Weisstein, 2016).

The above set of equations can be solved, and in the case of a turbulent flow, the solutions will display irregular motions in both space and time. At large length scales, these solutions will be subject to energy injection, while at small scales energy dissipation will occur (Brandenburg et al., 2012).

We now turn our attention to magnetized turbulence, which consists of fluctuations in the magnetic field of a source caused by an unstable build up of wave perturbations in the plasma (Galtier, 2009). These fluctuations can be classified as either isotropic, where the turbulence is the same in all directions, or anisotropic, where the turbulence is not the same in all directions (Houde et al., 2013). These turbulent regions will have extremely high magnetic Reynolds numbers up to 10^{13} and length scales ranging from a few metres up to 10^{18} m (Galtier, 2009).

1.4 Polarization

Electromagnetic waves propagate along a certain direction in space, but they also possess a direction of oscillation that is dictated by their polarization vector. These waves can exhibit various states of polarization characterized by varying states of linear and circular polarization. For example, if we consider a two dimensional wave that consists of the superposition of one horizontally polarized wave and one vertically polarized wave, we find a polarization vector that is given in terms of the polarization angle θ (eq. 1.3). The polarization angle represents the angle from the axis of oscillation relative to some predefined orientation. In the case of linear polarization, the horizontally and vertically polarized waves possess the same phase (Griffiths,

2013)

$$\hat{\boldsymbol{n}} = \cos\theta\,\hat{\boldsymbol{x}} + \sin\theta\,\hat{\boldsymbol{y}}. \tag{1.3}$$

There are several examples of polarization in astrophysics, such as the polarization of starlight by dust grain absorption (Ryden, B. and Peterson, 2010; Zeng, 2012) due to dust grain alignment caused by interstellar magnetic fields (Zeng, 2012). In the ionized plasma of a galaxy, the electrons gyrating around a magnetic field emit radiation that is polarized in the direction that is perpendicular to the magnetic field. This form of radiation is called synchrotron radiation (Mobilio et al., 2015).

1.5 Synchrotron Radiation

Synchrotron radiation occurs when relativistic electrons gyrating around magnetic fields lines in a source emit electromagnetic radiation. This radiation is polarized in the direction of the electron's acceleration, which is constantly changing due to the motion of the electron around the magnetic field but is perpendicular to the direction of the field. Cosmic sources, such as galaxies, are one example of emitters of synchrotron radiation (Schneider, 2006; Mobilio et al., 2015).

The number density of these electrons, in addition to the strength of the total magnetic field in the plane of the sky, determine the overall intensity of the emitted synchrotron radiation. In the case of linearly polarized synchrotron emission, the electrons interact with the ordered field that exists within the plane of the sky and the emitted radiation will not be completely polarized. The degree of polarization for linearly polarized synchrotron emissions in a regular field is given by equation (1.4), where α is the spectral index of synchrotron emission, and p_0 is the degree of polarization. For spiral galaxies, α is typically 0.8-1.0 so the maximum value for p_0 is approximately 73-75% (Beck, 2016)

$$p_0 = (1 + \alpha) \left(\frac{5}{3} + \alpha \right). \tag{1.4}$$

An ordered magnetic field will produce polarized synchrotron emission while unpolarized emission indicates the presence of a turbulent field (Beck, 2008, 2016).

1.6 Faraday Rotation

The direction of polarization vectors in a magnetized plasma is changed through the process of Faraday rotation. As Beck (2008) describes, the rotation angle is directly proportional to the density of the plasma, the strength of the field component that lies along the line of sight, and the square of the wavelength at which the data was observed. Faraday rotation can only be caused by regular magnetic fields, as the rotation angles are affected by the sign of the field direction. Measures of the Faraday rotation in combination with the total intensity of the synchrotron emission and polarization can provide a total picture of the mean magnetic field structure and direction in a galaxy.

1.7 Dispersion Analysis

1.7.1 The Dispersion Function

The magnetic field spanning the central region of IC 342 possesses a certain orientation in the plane of the sky. Since this field is turbulent, we can first model this using the angular structure function, which measures the difference in orientation of the magnetic field at two different points that are separated by a distance ℓ. The polarization angle at a certain measure of ℓ is measured by $\Phi(\ell)$ and the difference between two polarization angle measurements is given by $\Delta\Phi(\ell)$. The structure function itself is an average of the square of the difference between two polarization angle measurements for a given ℓ, which corresponds to $\langle \Delta\Phi^2(\ell) \rangle$ on the right hand side of equation 1.5. A hypothetical theoretical model of the angular structure function and its

statistically independent components can be found in panel a) of Figure 1.2. For simplicity, we then convert to the angular dispersion function, which is related to the angular structure function as follows:

$$1 - \langle \cos[\Delta\Phi(\ell)] \rangle \simeq \frac{1}{2} \langle \Delta\Phi^2(\ell) \rangle, \tag{1.5}$$

where $1 - \langle \cos[\Delta\Phi(\ell)] \rangle$ is the dispersion function and $\langle ... \rangle$ denotes an average.

The dispersion function contains both ordered and turbulent components that represent the ordered and turbulent components of the magnetic field, respectively. The ordered field varies over a large length scale while the turbulent component varies over a much smaller length scale. Since these components vary over different length scales and are statistically independent, we are able to separate them and analyze the turbulent component of the field.

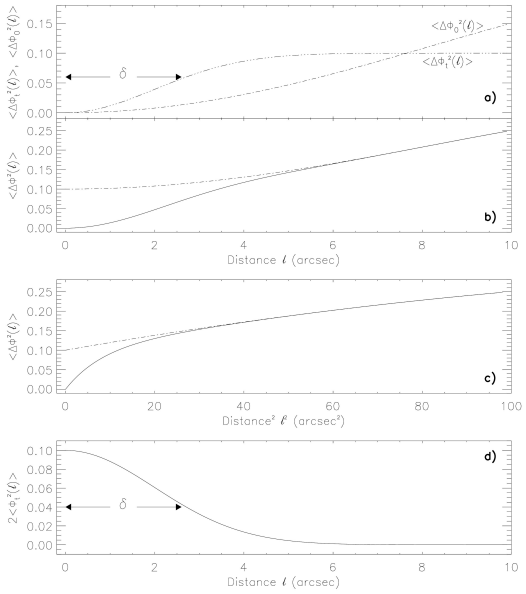

Figure 1.2: Theoretical models of the dispersion and autocorrelation functions. Panel (a) displays the hypothetical turbulent and ordered components of the structure function, while panel (b) displays the overall structure function. Panel (c) displays the structure function as well, but as a function of ℓ^2 rather than a function of ℓ. Panel (d) displays the turbulent autocorrelation function, which has been determined by subtracting the structure (or dispersion function) from a Taylor series fit for the ordered component obtained from its values at $\ell \geq 6$" (Houde et al., 2013).

1.7.2 The Autocorrelation Function

The subsequent components of the dispersion function can then be modelled by the autocorrelation function, which will contain the correlation length for the specified region in the galaxy. The autocorrelation function, shown below, is dependent upon both the correlation length and the telescope beam width; however, we are able to isolate the correlation length from the other variables to determine its exact value. The turbulence is assumed to be Gaussian, and in our case the specific form of the autocorrelation function models the isotropic turbulence. Under these assumptions the autocorrelation function takes the following form:

$$b^2(\ell) = \left[\frac{\langle B_t^2\rangle}{N\langle B_0^2\rangle + \langle B_t^2\rangle}\right] e^{-\ell^2/2(\delta^2+2W^2)} \tag{1.6}$$

where B_t^2 is the square of the turbulent field strength; B_0^2 is the square of the ordered field strength; δ is the correlation length for isotropic turbulence; W is the width of the telescope beam; and N is the number of turbulent cells in the column of gas probed by the telescope beam. The number of turbulent cells in isotropic turbulence is given by:

$$N = \frac{(\delta^2 + 2W^2)\Delta'}{\sqrt{2\pi}\delta^3} \tag{1.7}$$

where Δ' is the effective depth of the polarized gas that is probed by the telescope beam (Houde et al., 2013). A theoretical model of the turbulent autocorrelation function is presented in panel d) of Figure 1.2.

1.8 IC 342

IC 342 is a nearly face-on spiral galaxy that is approximately 3.5 Mpc away from us. After M31 and M33, it is the nearest spiral galaxy to the Milky Way (Beck, 2015). Every spiral galaxy has an inclination, which is the angle between the axis of rotation and the line of sight of the observer. This angle varies from 0° for a face-on spiral galaxy to 90° for an edge-on

spiral galaxy (Steinicke and Jakiel, 2007). According to Crosthwaite et al. (2000), IC 342 has an inclination of 31° relative to the plane of the sky.

Figure 1.3: Image of IC 342 taken by Mayall 4-meter telescope in 2006. Image credit: T.A. Rector/University of Alaska Anchorage, H. Schweiker/WIYN and NOAO/AURA/NSF.

IC 342 was studied in depth using synchrotron emission data by Beck (2015), but the first instance of linearly polarized emission being detected from the galaxy was by Krause (1987) using the VLA interferometer. A year later, Gräve & Beck (1988) used a combination of data from the Very Large Array (VLA) and Effelsberg telescopes to discern an ordered magnetic field in the galaxy. The VLA is a series of telescopes that collect data from radio sources. The data from each pair of telescopes in the configuration is combined to produce an interference pattern, which can be used to infer the structure of the radio source. This data can be used to produce maps by way of a Fourier transform (National Radio Astronomy Observatory, 2009).

The central region of IC 342 holds particular interest for a number of features in addition to the structure and strength of the magnetic field. In the center of the galaxy there is a bar of

dust and cold gas (Helfer et al., 2003), as well as evidence for starburst activity (Ishizuki et al., 1990). The starburst activity is not particularly recent due to a decreased star formation rate from stellar winds and supernova shocks (Schinnerer et al., 2008). A particular note of interest is that in terms of size, dynamical and molecular mass, and star formation rate, the nucleus of IC 342 could potentially be a twin of the Milky Way's galactic center (Meier, 2014).

In Figures 1.4 and 1.5 we display the data used in our analysis. Figure 1.4 shows a global view of the galaxy produced by the flux data obtained from VLA observations, while Figure 1.5 shows a closer view of the central region of the galaxy, which is the focus of our study. Figure 1.6 shows a map of the magnetic field in this central region overlaid on a map of CO emission in the region.

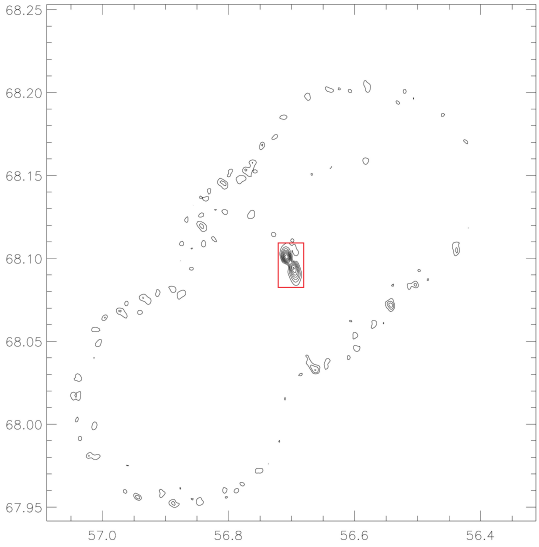

Figure 1.4: Global view of IC 342 provided by linearly polarized flux data at λ3.2 cm. The x and y axes are in units of degrees. The region used in the dispersion analysis is enclosed in a red box.

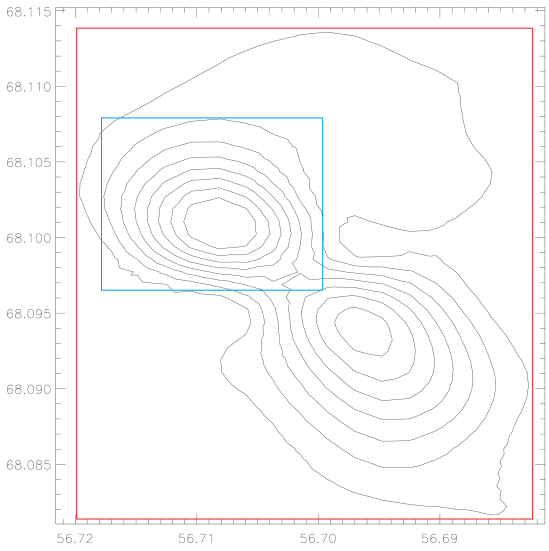

Figure 1.5: Map of polarized flux emission from central region of IC 342. The regions of study are indicated by the two coloured boxes on the plot, where the blue box indicates the inner lobe of the upper source, and the red box represents the entire source, with the exception of the aforementioned inner region that is removed from the analysis of the entire source. As in Figure 1.4, the x and y axes are in units of degrees.

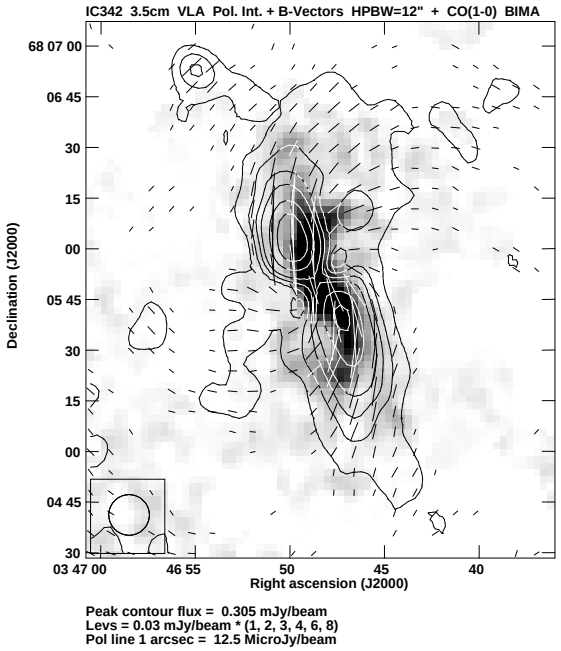

Figure 1.6: Linearly polarized intensity and observed B vectors in the central region of IC 342 at λ3.5cm at 12" resolution. This data has been overlaid on a greyscale presentation of the 2.6 mm CO emission in the region from the 2003 BIMA survey (Helfer et al., 2003). The x-axis is in units of arcseconds. Figure from Beck (2015).

1.9 Motivations and Goals

As stated in section 1.2, the origin of magnetic fields in galaxies remains undefined. Studying the properties of these fields, including their turbulence and its characteristics, may help to understand their evolution and shape future models of magnetic fields. In this thesis, we present the results of dispersion analysis performed on linearly polarized synchrotrom emission data from IC 342. The data and the computational programs used to perform the analysis are described in chapter 2. In chapter 3 we describe the results and present the relevant plots of the dispersion and autocorrelation functions. The discussion is presented in chapter 4 and concluding remarks in chapter 5.

Chapter 2

Methodology

2.1 Observations

We use previously published linearly polarized synchroton emission data that was collected using the VLA interferometer at λ3.5 cm. This data was attained from VLA maps that were combined and corrected for beam attenuation. The images were smoothed to a final resolution of 15" (Beck, 2015).

2.2 Dispersion Analysis in IDL

We used two IDL programs created by M. Houde to perform the dispersion analysis in the central region. Both of these programs were also used to characterize the magnetized turbulence in spiral galaxy M51 (Houde et al., 2013).

2.2.1 COSDISP Program

The first of these programs takes two FITS files, one that contains the polarization angle, and a second file that contains the polarization flux data. The program also requires a user-created parameter text file that describes the coordinates of the region to be analyzed. Once the program has read these three files, it organizes the data to determine the polarized flux and angle. The program then calculates the number of data points that will be used and produces

four images. These images show the relevant plots and images obtained from the data. They display the flux map of the galaxy, the contour plot of the region indicated by the positions dictated in the parameter file, a histogram of the polarization angle measurements, and the final image displays two plots, one of the dispersion function with respect to ℓ and a second plot of the dispersion function with respect to ℓ^2. All of the data created by this program is stored in a .out file that is then used as an input for the program ANGFITS.

2.2.2 ANGFITS Program

The second program takes the .out file produced by COSDISP containing the dispersion data, as well as a beam file that contains the beam profile, and the same parameter file used in the COSDISP program. Once the program has read the data, it then fits a low-order polynomial to the ordered component of the dispersion function, from which the data is subtracted to reveal the turbulent autocorrelation function. The program then fits a Gaussian function to the autocorrelation function and describes the fit of the Gaussian. This fit is used to determine the characteristic values of the magnetized turbulence, such as the correlation length, the number of turbulent cells, the intrinsic turbulent to ordered field ratio and the relevant uncertainties. Once these calculations are completed, the final plots are produced, which consists of two plots of the dispersion function and a plot of the turbulent autocorrelation function and Gaussian fit for both regions. These plots were created for both regions studied in the central region of IC 342 and can be found in chapter 3.

Chapter 3

Results

In order to investigate the distribution of the magnetized turbulence, we studied the inner region of the upper source and the entire source with the inner region removed. As indicated by Figure 1.5, we analyzed the inner upper source and then removed it from the entire source so that it was not included in the second analysis. We found that the inner region of the upper source contained no discernible correlation length, while the lower source and the outer region of the upper source contained notable turbulence and a distinct correlation length. In the following sections we will present our findings of these regions.

3.1 Inner Region of Upper Source

Our initial investigation of the upper source revealed the measured autorcorrelation function width was narrower than the width of the beam, which is not possible. However, expanding the search area around the upper source and allowing for data with flux values of at least 15 percent of the maximum revealed there to be additional data beyond our original search parameters. This revealed an additional region around the upper source. We adjusted the range of the beam to account for this area and conducted a new analysis, which revealed the presence of significant turbulence in the upper region. To study the turbulence in this area further, we divided the upper source into two regions: an inner region, where we expected there to be very little turbulence as per our previous results; and the outer region, where we expected to find

significant turbulence. We will review our findings of the inner portion here, while the outer portion will be discussed in the following section.

Using equations (1.5) and (1.6), we plot the dispersion function as a function of both ℓ and ℓ^2 as well as the turbulent autocorrelation function with respect to ℓ. The plots of the dispersion analysis results can be found in Figure 3.1.

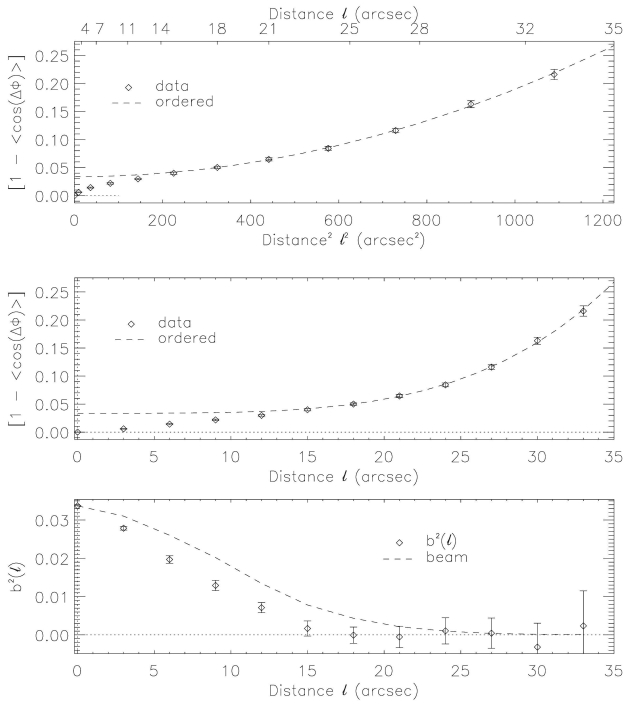

Figure 3.1: Dispersion analysis for the inner region of the upper source in the central region of IC 342. The top and middle panels display the dispersion function as function of ℓ^2 and ℓ respectively. The dotted 'ordered' line represents the least-squares fit for the sum of the turbulent-to-ordered magnetic energy ratio and the ordered component of the field to the data. The bottom panel shows the autocorrelation function that has been obtained by subtracting data from the fit in the middle plot. The dashed line represents the radial profile the "mean auto-correlated synthesized beam" (Houde et al., 2013). All data points are plotted with symbols.

The top plot shows the dispersion function plotted with respect to ℓ^2, while the middle plot also displays the dispersion function, but it is plotted with respect to ℓ rather than ℓ^2 to show the difference between the ordered fit and the data. The curves labelled 'ordered' in the top and middle plots represent the least-squares fit that has been calculated with respect to the integrated turbulent-to-total magnetic energy ratio, which is represented by equation (1.6) when ℓ is equal to zero. The integrated turbulent autocorrelation function, which is determined by

subtracting the data from the least-squares fit, is shown in the bottom plot. The "autocorrelated synthesized beam" plotted with the data in the bottom panel represents the contribution of the synthesized beam to the width of the function. More specifically, it represents the plot of $b^2(\ell)$ when the correlation length δ is equal to zero.

The dispersion analysis performed on the upper internal region of the central source revealed that the width of the autocorrelation function is significantly narrower than the width of the autocorrelated beam. Additionally, the plot of the dispersion function has a small y-intercept, indicating that there is little turbulence measured in the region. However, since the correlation length is narrower than the beam, we cannot accurately determine the number of turbulent cells or a ratio for the turbulent to ordered field strength and thus cannot analyze the region any further.

3.2 Entire Source

By removing the inner lobe of the upper source, we allow the program to analyze the sections of the entire region that we know contain significant turbulence. This allows us to get an overall picture of the turbulence in the entire central region of the galaxy, as shown in Figure 1.5. Figure 3.2 shows the results of this analysis.

We found the turbulent correlation length for this region to be 8.5 ± 0.5", or 144 ± 9 pc using the estimates of IC 342's distance from Beck (2015). Since we were able to determine a correlation length for this region, we were also able to determine estimates for the number of turbulent cells, the integrated turbulent-to-total energy ratio and the turbulent-to-ordered field ratio. These results are presented in Table 3.1.

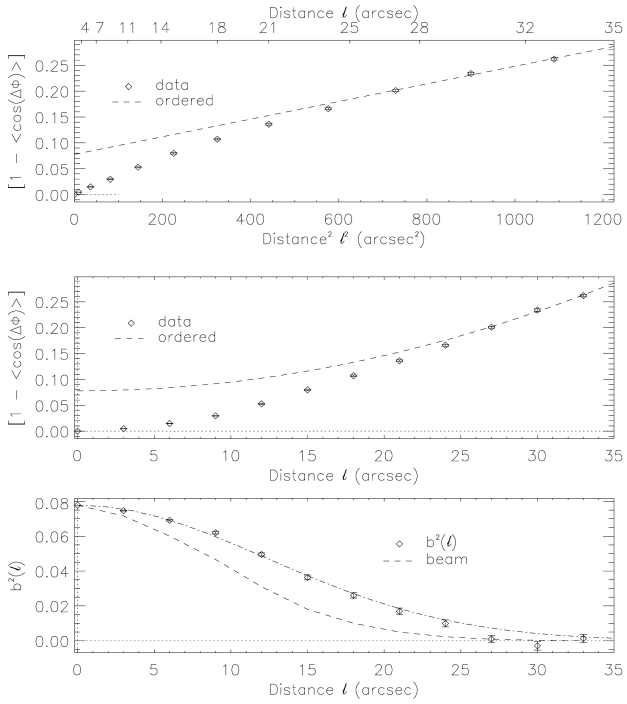

Figure 3.2: Dispersion Analysis for the entire central region in IC 342 with the upper inner region removed. The broken dashed line in the bottom panel represents the Gaussian fit. The same fits and program were used to produce these plots as were used for Figure 3.1.

	Entire Central Source
δ(pc)^{i}	144 ± 9
N^{ii}	6 ± 1
$\langle\overline{B}_t^2\rangle/\langle\overline{B}^2\rangle^{iii}$	0.078 ± 0.013
B_t/B_0^{iv}	0.70 ± 0.04

Table 3.1: Table I: Results of dispersion analysis for turbulent regions in the center of IC 342.
i. The turbulent correlation length, calculated using 1" = 17 pc.
ii. Number of turbulent cells using $\Delta' = 1000$ pc.
iii. Integrated turbulent-to-total magnetic energy ratio.
iv. Intrinsic ratio of the turbulent-to-ordered field strength.

Chapter 4

Discussion

A similar analysis was performed on the galaxy M51 by Houde et al. (2013) using the same method of dispersion analysis. If we compare our values of correlation length, number of turbulent cells, integrated turbulent-to-total magnetic energy ratio, and the ratio of the turbulent-to-ordered field strength, we note some similarities and differences between the characteristics of the magnetized turbulence in the two galaxies. In the case of isotropic turbulence, Houde et al. (2013) were able to discern characteristics for the magnetized turbulence in M51 for the center and southwest arm of the galaxy. In both cases the determined correlation length for these regions is approximately half of the correlation length found for the center of IC 342.

Our result for the number of turbulent cells in the central region of IC 342 is approximately half the number of turbulent cells found in M51, which is a direct result of the larger correlation length in IC 342. According to equation (1.7), a greater correlation length will correspond to a smaller number of turbulent cells because of the δ^3 term that dominates in the denominator of the equation.

The integrated turbulent-to-total magnetic energy ratio for the central region of IC 342 is similar to the values of 0.088 and 0.072 found for the center and southwest arm of M51, re-

spectively.

A notable difference between our findings and those of Houde et al. (2013) is that the ratio of the turbulent-to-ordered field strength for both the center and southwest arm in M51 is greater than the ratio determined for the central region of IC 342. The field strength ratios for the center and southwest arm of M51 are 1.13 and 1.04, respectively, while for IC 342 we found a field strength ratio of 0.70. The difference in these ratios suggests that IC 342 has a relatively stronger ordered field than M51.

As noted by Beck (2015) and seen in Figure 1.6, the magnetic field is ordered about the 'double-lobe' formation in the center of IC 342. The galaxy rotates in a counter-clockwise fashion, causing the ordered field to be strongest in the regions that follow the CO bar in its rotation. Beck (2015) also notes that the degree of polarization in the upper source is approximately 8%, twice the degree of polarization ($\approx$4%) in the lower source. These low polarization levels suggest the presence of unpolarized synchrotron emission, which arises from isotropic turbulent or tangled fields (Beck, 2016).

If we consider the orientation of the field vectors in the entire central region relative to the position of the CO bar (Figure 1.6), we note that the strongest ordered field components are in the southern and northeastern regions of the center of IC 342, which is caused by tracings of the flow patterns in the central region (Beck, 2015). The location of these ordered field components and their strength agrees with our results as our turbulent-to-ordered field strength ratio in the entire central source suggests there to be a strong ordered magnetic field in the region. As the field approaches the CO bar, the field vectors form a spiral pattern with large pitch angles, possibly caused by mean-field dynamos (Beck, 2015).

Though we were able to successfully determine characteristic values for the entire central

region of IC 342, we must also acknowledge the shortcomings present in our methods. As noted by Houde et al. (2013), the resolution of the data used can have a large impact on the results determined. If the resolution of the data is not high enough, then it becomes difficult to separate the small and large-scale components from one another. This may be the cause for the undetermined correlation length in the internal region of the upper source, as a particularly small correlation length scale could easily become lost in the data if the resolution is not sufficiently high. Additionally, if the resolution of the data is high enough we can use the beam broadened turbulent autocorrelation function to determine the turbulent power spectrum of the field by means of a Fourier transform. However, the resolution of our data was not high enough to complete this.

It is also worth noting that we only performed a dispersion analysis for the isotropic field, which is likely an idealization of the state of the magnetic field in IC 342. In reality the field is likely perturbed with shocks from supernovae and other injectors of kinetic energy, which would cause anisotropy in the field. The anisotropic case is also a more general model of the magnetized turbulence, whereas the isotropic case is a specific form of the magnetized turbulence with a single turbulent correlation length scale, rather than two separate correlation length scales that are parallel and perpendicular to the local ordered magnetic field, respectively (Beck, 2015). The anisotropic case will also require additional data because it evolves into a two-dimensional problem due to the anisotropy.

Chapter 5

Conclusions

5.1 Concluding Statements

We performed a dispersion analysis on previously published $\lambda 3.5$ cm linearly polarized synchrotron emission data from using computational programs developed by Houde et al. (2013) to characterize the magnetized turbulence in the central region of IC 342. We analyzed two regions in the center of the galaxy: the internal region of the upper source and the entire central source with the upper internal region removed. We determined a turbulent correlation length of 144 ± 9 pc for the entire central source, which differs from the results reported by Houde et al. (2013) for the center of M51 but is still reasonable. We also determined a turbulent-to-ordered field ratio for the entire central source of 0.70 ± 0.04, which is less than the value reported for M51 and is likely due to a stronger ordered component in the magnetic field of IC 342.

5.2 Future Work

The next steps in the analysis of the magnetic field in IC 342 would be to test for anisotropy in the field in the central region, which would be indicated by a difference in the parallel and perpendicular correlation lengths that arise from anisotropy in the field. Additionally, higher resolution data should be sought to complete a more rigorous analysis that could also yield a turbulent power spectrum of the data.

Bibliography

Beck, R. (2008), 'Measuring interstellar magnetic fields by radio synchrotron emission', *Proceedings of the International Astronomical Union* **4**(S259).

Beck, R. (2015), 'Magnetic Fields in the nearby spiral galaxy IC 342: A multi-frequency radio polarization study', *Astronomy & Astrophysics* **578**(A93).

Beck, R. (2016), 'Magnetic fields in spiral galaxies', *The Astronomy and Astrophysics Review* **24**(1).

Bertone, S., Vogt, C. and Enßlin, T. (2006), 'Magnetic field seeding by galactic winds', *Monthly Notices of the Royal Astronomical Society* **370**.

Brandenburg, A., Sokoloff, D. and Subramanian, K. (2012), 'Current Status of Turbulent Dynamo Theory: From Large-Scale to Small-Scale Dynamos', *Space Science Reviews* **169**(1).

Crosthwaite, L. P., Turner, J. L. and Ho, P. T. P. (2000), 'Structure in the Neutral Hydrogen Disk of the Spiral Galaxy IC 342', *The Astronomical Journal* **119**(4).

Furlanetto, S. and Loeb, A. (2001), 'Intergalactic Magnetic Fields From Quasar Outflows', *The Astrophysical Journal* **556**.

Galtier, S. (2009), 'Wave turbulence in magnetized plasmas', *Nonlinear Processes in Geophysics* **16**(1).

Griffiths, D. J. (2013), *Introduction to Electrodynamics Fourth Edition*, Pearson Education Inc.

Hanayama, H., Takahashi, K., Kotake, K., Oguri, M., Ichiki, K. and Ohno, H. (2005), 'Biermann Mechanism in Primordial Supernova Remnant and Seed Magnetic Fields', *The Astrophysical Journal* **633**(2).

Helfer, T. T., Thornley, M. D., Regan, M. W., Wong, T., Sheth, K., Vogel, S. N., Blitz, L. and Bock, D. C. J. (2003), 'The bima survey of nearby galaxies (bima song). ii. the co data', *The Astrophysical Journal Supplement Series* **145**(2).

Houde, M., Fletcher, A., Beck, R., Hildebrand, R., Vaillancourt, J. and Stil, J. (2013), 'Characterizing Magnetized Turbulence in M51', *The Astrophysical Journal* **766**(49).

Ishizuki, S., Kawabe, R., Okumura, S. K., Morita, K.-I. and Ishiguro, M. (1990), 'Co mapping of the nuclear region of ngc 6946 and ic 342 with nobeyama millimeter array', *Nature* .

Krause, M. (1987), Magnetic field structures in 1181 and ic 342, *in* 'Magnetic fields and extragalactic objects: proceedings of an international workshop, held May 31th [sic]-June 6th, 1987 at" Institut d'Etudes Scientifiques de Cargèse", Corse du Sud, France', Distributor," Editions de Physique", p. 171.

Kulsrud, R., Cowley, S., Gruzinov, A. and Sudan, R. (1997), 'Dynamos and cosmic magnetic fields', *Physics Reports* **283**(1-4).

Meier, D. S. (2014), 'The nucleus of ic 342 as a potential twin of the galactic center', *International Astronomical Union. Proceedings of the International Astronomical Union* **9**(S303), 66–68.

Miranda, O., Opher, M. and Opher, R. (1998), 'Seed magnetic fields generated by primordial supernova explosions', *Monthly Notices of the Royal Astronomical Society* **301**(2).

Mobilio, S., Boscherini, F. and Meneghini, C. (2015), *Synchrotron Radiation: Basics, Methods and Applications*, Springer Berlin Heidelberg.

Moss, D. (2012), 'Modelling magnetic fields in spiral galaxies', *Astronomy & Geophysics* **53**(5).

National Radio Astronomy Observatory (2009), 'An Overview of the Very Large Array'. http://www.vla.nrao.edu/genpub/overview/.

Phillips, S. (2005), *The Structure and Evolution of Galaxies*, John Wiley & Sons Ltd.

Ryden, B. (2011), 'Astronomical Gas Dynamics: Chapter 7'. http://www.astronomy.ohio-state.edu/~ryden/ast825/ch7.pdf.

Ryden, B. and Peterson, B. M. (2010), *Foundations of Astrophysics*, Pearson Addison-Wesley.

Ryu, D., Kang, H. and Biermann, P. (1998), 'Cosmic magnetic fields in large scale filaments and sheets', *Astronomy & Astrophysics* **335**.

Schinnerer, E., Böker, T., Meier, D. S. and Calzetti, D. (2008), 'Self-regulated fueling of galaxy centers: Evidence for star formation feedback in ic 342s nucleusbased on observations carried out with the iram plateau de bure interferometer. iram is supported by insu/cnrs (france), mpg (germany), and ign (spain).', *The Astrophysical Journal Letters* **684**(1), L21.

Schneider, P. (2006), *Extragalactic Astronomy and Cosmology: An Introduction*, Springer Berlin Heidelberg.

Sparke, L. and Gallagher III, J. (2007), *Galaxies in the Universe: An Introduction*, Cambridge University Press.

Steinicke, W. and Jakiel, R. (2007), *Galaxies and How to Observe Them*, Springer Verlag London Limited.

Tsagas, C. (2005), 'Resonant amplification of magnetic seed fields and gravitational waves in the early universe', *Physical Review D - Particles, Fields, Gravitation and Cosmology* **72**.

Wagstaff, J., Benerjee, R., Schleicher, D. and Günter, S. (2014), 'Magnetic field amplification by the small-scale dynamo in the early Universe', *Physical Review D* **89**.

Weisstein, E. (2016), 'Navier-stokes equations'. http://mathworld.wolfram.com/Navier-StokesEquations.html.

Widrow, L., Ryu, D., Schleicher, D., Subramanian, K., Tsagas, C. and Treumann, R. (2012), 'The First Magnetic Fields', *Space Science Reviews* **166**(1).

Xu, H., Li, H., Collins, D., Shengtai, L. and Norman, M. (2010), 'Evolution and Distribution of Magnetic Fields from Active Galactic Nuclei in Galaxy Clusters. I. The Effect of Injection Energy and Redshift', *The Astrophysical Journal* **725**.

Yu, J. (2012), 'Lecture 4: Circulation and Vorticity'. http://www.ess.uci.edu/~yu/class/ess228/lecture.4.vorticity.all.pdf.

Zeng, L. (2012), 'Polarimetry in astrophysics and cosmology'. http://uwo.summon.serialssolutions.com/2.0.0/link/0/eLvHCXMwY2AwNtIz0EUrE5INk0EVoXGiYVqSSaplGrAbYWlimZySaA5qcaQkoZ2ZBLvCFRrbsEISXHKn5CeDBs31gU0ZYFPECJiG7AsKdU\HXSIGmW2F3aiRC71pIAWZpQ9AmdFYjYN8dlOzdkdtH8O68oZGZuTmwLQI5J9DcAs43xCikwTWPmwBDA2z_DnQtNuxcJ1ivNrWqILG0JAP\SqUU63ZFqnhJk4HFBmrQXYmBKzRNh0AwA9Ykzc1NLiioVMvMUEotLivIhwyTFCol5KQrJ-cW54CF7UQZlN9cQZw9dmFPioem3OB7hDmMxBl6\QN0Brl0BrtFIkGBTMDVOAZZNZcrKhaaKJuUFykkGqRWIyaELRONnI3ChJkkEGn5FS-KWlGbiArRIjyDiHDANLSVFpqiy45gcAGlOziA.